

The Heliosphere as Seen in TeV Cosmic Rays

Ming Zhang

Department of Physics and Space Sciences, Florida Institute of Technology,
Melbourne, Florida 32901, USA

E-mail: mzhang@fit.edu

Nikolai Pogorelov

Center for Space Plasma and Aeronomic Research and Department of Space
Sciences, University of Alabama in Huntsville, Huntsville, Alabama 35899, USA

Abstract. Measurements from several cosmic-ray air shower experiments reveal that the anisotropy of TeV cosmic-ray flux does not agree with a dipole pattern commonly expected from the Compton–Getting effect or from the diffusion of cosmic rays in Galactic magnetic fields. TeV cosmic-ray anisotropy maps often show fine features, some of which are slightly time-dependent. Because the size of the heliosphere is larger than the gyroradius of TeV cosmic rays in the interstellar magnetic field, the electric and magnetic fields of the heliosphere may distort the pattern of cosmic-ray anisotropy that one would see in the local interstellar medium without the presence of the heliosphere. We have developed a method of mapping cosmic-ray anisotropy using Liouville’s theorem. In this paper, we show how to use cosmic-ray anisotropy features to determine the direction of the local interstellar magnetic field, the hydrogen deflection plane, the size and shape of the heliotail, and the geometry of the heliosphere bow wave.

1. Introduction

The directional variation (anisotropy) in the intensity of TeV cosmic rays arriving at Earth is routinely measured by a number of air shower experiments, such as Tibet AS γ , IceCube, Super-Kamiokande, Milagro, ARGO-YBG, HAWC and many others [1], [2], [3], [4], [5], [6], [7], [8], [9], [10]. In the last decade, the data quality and event statistics from these experiments have reached a level that can decisively determine the anisotropy and its variation better than 10^{-4} . Surprising features are revealed. At several TeV energies, although there is an overall large-scale pattern of dipole anisotropy with an amplitude of $\sim 10^{-3}$, small (a few degrees) to medium (tens degrees) scale angular structures are clearly visible. Some small scale features are slightly time-dependent too (e.g., [1]). The small-scale structures, which are often referred to as hot spots [3], [4], become more evident in lower energies of around 1 TeV. The overall dipole orientation and amplitude



do not agree with the Compton–Getting effect from the motion of the heliosphere relative to the local interstellar medium at ~ 25 km/s. What is more puzzling is that the large-scale anisotropy is energy-dependent. At high energies greater than a few hundred TeV, the direction of dipole anisotropy is opposite to that at a few TeV energies ([6], [7], [8]).

A number of authors have tried to interpret TeV cosmic-ray anisotropy measurements using various mechanisms (e.g., [11], [12], [13], [14], [15]). It was also suggested in [16] and [17] that it is the heliosphere that contributes to the observed anisotropy. This is expected because the gyroradius of TeV cosmic rays in an average $3\mu\text{G}$ interstellar magnetic field is less than the size of the heliosphere, so their trajectories are altered by the heliospheric magnetic and electric fields, resulting in distortion to the pattern in the original interstellar space.

In this paper, we concentrate on using the measurements of TeV cosmic-ray anisotropy to explore the magnetic structures of the heliosphere. After presenting our theory of mapping cosmic-ray anisotropy using Liouville’s theorem, we show our calculation results trying to match features in the measured map of cosmic-ray anisotropy obtained by the Tibet AS γ experiment. We identify the features of anisotropy related to our choice of the BV -plane (the plane determined by the magnetic field and velocity vectors in the unperturbed interstellar medium), the plane perpendicular to the local interstellar magnetic field, the heliotail, and the heliospheric bow wave. The bow wave is defined as the region of the interstellar plasma that is affected by the presence of the heliosphere [21]. Note also that our BV -plane is always close to the hydrogen deflection plane (HDP), which is determined by the H-atom velocity vectors in the unperturbed interstellar medium and in the inner heliosphere as determined in the *SOHO* Solar Wind Anisotropy experiment [20].

2. Models

2.1. Liouville mapping of anisotropy

At a fixed energy, the cosmic-ray flux measured by an experiment on Earth is proportional to the particle distribution function in Earth’s frame of reference. According to Liouville’s theorem, the distribution function is conserved along particle trajectories, and it is also conserved upon Lorentz transformation of reference frames, that is:

$$f(\mathbf{r}_o, \mathbf{p}_o) = f(\mathbf{r}, \mathbf{p}) \quad (1)$$

where $f(\mathbf{r}_o, \mathbf{p}_o)$ is in the Earth frame and $f(\mathbf{r}, \mathbf{p})$ is in the local interstellar medium. Liouville’s theorem is valid as far as one can fully determine the particle trajectory.

The distribution function of cosmic rays in the local interstellar medium is not known, although we have a reasonably good knowledge about its energy dependence. This is because the spatial and angular dependence of cosmic-ray distribution in the interstellar medium is sensitive to the history of nearby supernova sources in the past few million years. These dependences are likely to be a function of particle energy, as cosmic-ray interstellar propagation is energy-dependent. Lacking direct measurements, we assume the following distribution function for cosmic rays in the local interstellar medium:

$$f(\mathbf{r}, \mathbf{p}) = f_0 p^{-\gamma} \left[1 + \nabla_{\perp} \ln f \cdot (\mathbf{R}_g - \mathbf{r}_0) + A_{||1} P_1(\mu) + A_{||2} P_2(\mu) \right] \quad (2)$$

where p is the magnitude of \mathbf{p} , \mathbf{R}_g is the location of particle guiding center (one gyroradius vector away from \mathbf{r}), $P_1(\mu)$ and $P_2(\mu)$ are the first and second Legendre polynomials of particle pitch angle cosine μ with respect to the magnetic field. Other symbols in Eq (2) are constants: $A_{||1}$ and $A_{||2}$ are the amplitudes of pitch angle anisotropies, $\nabla_{\perp} \ln f$ is the cosmic-ray density gradient perpendicular to the magnetic field, and $\gamma \approx 4.75$ is the slope of cosmic-ray power-law energy distribution. Since TeV cosmic rays in the interstellar medium are sufficiently magnetized and scattered on the Galactic scale, the distribution function in the interstellar plasma frame of reference is nearly isotropic, so the spatial dependence and pitch-angle dependence is small, thus qualifying it be written in the above perturbation form. The energy dependence gives rise to the Compton–Getting anisotropy due to the transformation of reference frames, and it also includes the effect of particle acceleration during its propagation through the heliosphere. The guiding center dependence contains the cross gradient anisotropy and the particle drift effect [16]. The pitch-angle dependence is related to cosmic-ray diffusion parallel to the average magnetic field and possible mirroring by the interstellar magnetic field on the Galactic scale. The values of constants $A_{||1}$, $A_{||2}$ and $\nabla_{\perp} \ln f$ control the contribution from these three types of anisotropy sources. Since we do not know the past history of cosmic rays arriving at Earth, these four constants are free parameters to be determined by fitting cosmic-ray anisotropy measurements with models.

2.2. Heliospheric propagation of cosmic rays

The cosmic-ray trajectory can be calculated using Newton’s equation with the Lorentz force. The trajectory can be fully determined once the total magnetic and electric fields are known. We use a multi-fluid MHD heliospheric model implemented in the Multi-Scale Fluid-Kinetic Simulation Suite (MS-FLUKSS) [22, 23]. It addresses the complexity of the charge-exchange processes between solar wind ions and interstellar neutrals and coupling between the interstellar and heliospheric magnetic fields (e.g., [18]). Table 1 lists parameters used to simulate the heliosphere model. Among the outputs of the MHD model are plasma velocity \mathbf{V} and magnetic field \mathbf{B} . In ideal MHD, electric field can be calculated with $\mathbf{E} = -\mathbf{V} \times \mathbf{B}$. Note that the fields from MHD solution are average fields, which only reveal large-scale heliospheric structures. In space plasma, there is always a random fast, small-scale field component. For TeV cosmic rays, scattering by magnetic fluctuations is slow, in the order of one scattering every a few years to match their mean free path of a few pc in the interstellar medium, while the particle propagation through the heliosphere of a few thousand AU size is just tens of days. So the transport through the heliosphere is essentially scatter-free in the average fields.

Once the momentum at Earth $\mathbf{p}_o(\mathbf{r}_o)$ is mapped in time backward to the interstellar medium at far enough distance $\mathbf{p}(\mathbf{r})$ for all directions of \mathbf{p}_o viewed from Earth, maps of anisotropy due to all variables in the distribution functions are obtained. According to Eq (2), the composite map is basically a linear combinations of anisotropy maps produced by three anisotropy mechanisms. We do least χ^2 fit to observations of relative cosmic-ray fluxes to determine the free constants in Eq (2).

3. Results

The top panel of Figure 1 shows a map of cosmic-ray relative flux at 5 TeV measured by the Tibet AS γ experiment as a function of declination and right ascension [19]. On the large scale, the cosmic-ray flux shows an enhancement in the tail region and a deficit in the nose region. The middle panel is our model fit with the constants listed in Table 2. In our calculation, Earth is set to be stationary, which corresponds to a yearly average of cosmic-ray anisotropy. A number of features in our model match the observations quite well, except the locations of some boundaries are shifted a little bit due to the uncertainties about the interstellar magnetic field, ion and neutral densities used in our MHD heliosphere simulation. The bottom panel, calculated from Eq (2) without the heliospheric particle propagation, is an inferred map of cosmic-ray anisotropy as would be seen in the local interstellar medium without the presence of the heliosphere. Notice in Table 2, the amplitude of first order pitch-angle anisotropy $A_{||1}$ is much larger than the other two constants, indicating that the interstellar cosmic-ray anisotropy is dominated by diffusion along the magnetic field. $A_{||1}$ is positive, meaning higher cosmic-ray flux at zero pitch angle to the interstellar magnetic field than in the opposite direction. To the zeroth order, the overall dipole pattern in the observation comes from the original interstellar cosmic-ray anisotropy of the bottom panel. The magnetic and electric fields of the heliosphere distort the original interstellar anisotropy map. The amount of distortion can be seen directly by subtracting the interstellar anisotropy from the observation or from our model fit. Figure 2 shows a comparison between them. Although some boundaries are shifted slightly, the patterns in the observed distortion and the model distortion match very well. This suggest that the heliosphere model we have used is quite good in describing the large-scale heliospheric structures.

Let us exam a few features of cosmic-ray anisotropy in Figure 1 and their heliospheric origin. The cosmic-ray flux is enhanced in the tail direction narrowly aligned with the hydrogen deflection plane [20], which coincides with the plane containing the interstellar flow and magnetic field vectors in our heliosphere model. The surface of the heliopause in the tail region is also elongated along the hydrogen deflection plane. In the directions of flux enhancement, cosmic-ray trajectories are focused by the magnetic field in the heliotail or their pitch angles before entering the heliosphere are close to zero degree from the interstellar magnetic field. Slightly outside of the flux enhancement, particularly on the right-hand side, the cosmic-ray flux is dramatically reduced from its original interstellar level (the blue region on the right side of Figure 2). There, the cosmic rays are defocused by the magnetic field of the outer heliosheath. These cosmic rays originally come in with larger original pitch angles. On the other side centered around the right ascension 300° , cosmic-ray flux is enhanced by the heliospheric distortion (the red region on the left side of Figure 2). Thses cosmic rays drift in the direction opposite to the cosmic-ray density gradient when they pass through the outer heliosheath, and they have higher densities originally in the interstellar medium.

The blue region of cosmic-ray flux deficit in Figure 1 is confined roughly around the nose direction. These cosmic rays originally have pitch angles close to 180° to the interstellar magnetic field, in which direction the original interstellar cosmic-ray flux is near the lowest. In our model simulation, the cosmic-ray flux distribution in this flux deficit (blue) region is relatively smooth. This is because these cosmic rays

pass through a thinner part of the heliosheath and solar wind, and their trajectories are not very much complicated by the inhomogeneity of the magnetic field due to the short propagation. To the right, the blue region in Figure 1 is approximately bounded by the plane perpendicular to the unperturbed interstellar magnetic field. Inside the blue region, cosmic rays come from the nose side with large pitch angles $> 90^\circ$ and outside they come from the tail direction with small pitch angle $< 90^\circ$. Apparently, the magnetic field in the solar wind and heliosheath along the trajectories of these particles do not deflect the cosmic-ray trajectories very much. Comparing the location of this boundary in our simulation with what is observed by Tibet AS γ , we probably can say that magnetic field direction we used in our heliosphere simulation should be quite close to the true interstellar magnetic field direction. On the left side, the boundary of the blue region in Figure 1 also separates the cosmic rays coming from the nose direction from those coming from the tail direction. However, it is far away from the plane perpendicular to the interstellar magnetic field on that side. This is because these cosmic-ray trajectories are strongly deflected by the heliosheath and heliotail magnetic field. Detailed examination of the trajectories of particles arriving in the directions on the both sides of this boundary (Figure 3) shows that the trajectories are separated by the bow wave in front of the heliosphere. Particle coming from the nose can quickly arrive at Earth, but the particles from the tail direction are severely deflected by the draped interstellar magnetic field in the outer heliosheath and heliospheric magnetic field in the heliotail, and they eventually arrive in the directions close to the nose. The precise location of this boundary in our model calculation is somewhat off from what is observed. Perhaps, this is due to our boundary conditions, which are essentially taken from [24], or maybe our multi-fluid approach does not describe the formation of the bow wave with enough precision. In order to better fit the observations, the bow wave of future models should either move outward or have a larger angle between the bow wave surface and the interstellar flow. In either case, the Mach number (most likely, fast magnetosonic) should be further reduced, which requires that the (magnetosonic) wave speed should be larger than in the current simulation.

In Figure 1, the middle panel of our model calculation demonstrates some spots of cosmic-ray enhancements at high declinations of $> 60^\circ$. The Tibet AS γ observations in Figure 1 top panel do not show the feature. So the enhancements in the model results must be artifacts of our model. If we reduce the size of MHD simulation box by replacing the magnetic field and plasma parameters outside of 2000 AU (in the second circle in Figure 3) with those in the pristine interstellar medium, we find that the artifacts become more obvious (Figure 4). Examination of the trajectories of particles arriving in the direction of the artifacts shows that cosmic rays originally come from the heliotail and the magnetic field at high northern declinations of the heliosheath deflects them southward. From this analysis we conclude that the heliosphere, particularly the heliotail, has to be long, probably more than the maximum of 4400 AU in our MHD simulation.

4. Conclusion and discussion

The heliosphere can distort the map of cosmic-ray anisotropy originated in the local interstellar medium due to the energy, spatial and pitch-angle dependence of the cosmic-ray distribution function. We have used Liouville’s theorem to map the interstellar

cosmic-ray anisotropy to Earth. The measured map of 5 TeV cosmic-ray anisotropy obtained by the Tibet AS γ experiment suggests that the cosmic-ray anisotropy in the local interstellar medium is dominated by a dipole resulted from cosmic-ray diffusion parallel to the magnetic field, although there contain weaker contributions from the Computon-Getting effect, cosmic-ray density gradient, mirroring by interstellar magnetic field inhomogeneity. We have identified a few features of cosmic-ray anisotropy caused by heliospheric magnetic field structures. These feature can be used to locate the hydrogen deflection plane, the plane perpendicular to interstellar magnetic field, and the heliospheric bow wave.

The measured map of cosmic-ray anisotropy also contains many small-scale variations. Some of them around the ecliptic could be caused the coronal or inner heliospheric magnetic fields. Those far way from the ecliptic must come either for the large-scale interstellar magnetic turbulence or for the heliospheric magnetic field variation in the heliotail region. It is possible we can use these small-scale variations to probe the properties of these magnetic field fluctuations. The original source of all anisotropies is the variation of cosmic-ray distribution function in the pristine interstellar medium. Only when the original interstellar anisotropy is fully figured out can we uniquely decode out the properties of magnetic field fluctuations.

4.1. Acknowledgments

This work was supported in part by NSF Grant AGS-1156056, NASA Grants NNX14AJ53G, NNX15AN72G, and NNX15AB76G, and DOE Grant DE-SC0008721. This work was also partially supported by the IBEX mission as a part of NASA’s Explorer program. We acknowledge NSF PRAC award OCI-1144120 and related computer resources from the Blue Waters sustained-petascale computing project. Supercomputer time allocations were also provided on SGI Pleiades by NASA High-End Computing Program award SMD-15-5860 and on Stampede by NSF XSEDE project MCA07S033.

5. References

- [1] Amenomori, M., Ayabe, S., Bi, X. J., et al. 2006, *Science*, 314, 439
- [2] Amenomori, M., Ayabe, S., Bi, X. J., et al. 2010, *Astrophys. J.*, 711, 119
- [3] Abdo, A. A., Allen, B. T., Aune, T., et al. 2008, *Phys. Rev. Lett.* 101, 221101
- [4] Abdo, A. A., Allen, B. T., Aune, T., et al. 2009, *ApJ*, 698, 2121
- [5] Guillian, G., Hosaka, J., Ishihara, K., et al. 2007, *Phys. Rev. D*, 75, 062003
- [6] Abbasi, R., Abdou, Y., Abu-Zayyad, T., et al. 2010, *Astrophys. J.*, 718, L194
- [7] Abbasi, R., Abdou, Y., Abu-Zayyad, T., et al. 2011, *Astrophys. J.*, 740, 16
- [8] Abbasi, R., Abdou, Y., Abu-Zayyad, T., et al. 2012, *Astrophys. J.*, 746, 33
- [9] Di Sciascio, G., Iuppa, R., Argo-Ybj Collaboration, 2012, *J. Phys.: Conf. Ser.*, 375, 052008
- [10] Abeysekara, A. U., Alfaro, R., Alvarez, C., et al. 2014, *Astrophys. J.*, 706, 108
- [11] Drury, L. O.C. and Aharonian, F. A., 2008, *Astroparticle Physics* 29, 420.
- [12] Lazarian, A., and Desiati, P., 2010, *Astrophys. J.*, 722, 188
- [13] Giacinti, G., and G. Sigl, 2012, *Phys. Rev. Lett.*, 109, 071101.
- [14] Desiati, P., & A. Lazarian 2013, *Astrophys. J.*, 762, 44.
- [15] K. Kotera, M. Perez-Garcia and J. Silk, arXiv:1303.1186
- [16] Zhang, M., Zuo, P., Pogorelov, N., 2014, *Astrophys. J.*, 790, 5.
- [17] Schwadron, N.A., et al. 2014, *Science*, 1245026.
- [18] Pogorelov, N., et al., 2015, *Astrophys. J. Lett.*, 812, L6.
- [19] Amenomori, M., et al. 2011, *Proc. 32nd ICRC*, 1, 62.

- [20] Lallement, R. et al., 2005, Science, 307, 1447.
- [21] Zank, G. P., Heerikhuisen, J., Pogorelov, N.V., Burrows, R., McComas, D., 2010, Astrophys. J., 708, 1092
- [22] Pogorelov, N. V., Borovikov, S. N., Bedford, M. C., Heerikhuisen, J., Kim, T. K., Kryukov, I. A., Zank, G. P. 2013, in ASP Conf. Proc. Ser. 474, Numerical Modeling of Space Plasma Flows (ASTRONUM-2012), eds. N.V. Pogorelov, E. Audit, and G. P. Zank, 165 (Astron. Soc. Pacific, San Francisco)
- [23] Pogorelov, N. V., Borovikov, S. N., Heerikhuisen, J., Kim, T. K., Kryukov, I. A., Zank, G. P. 2014, in XSEDE'14: Proceedings of the 2014 Annual Conference on Extreme Science and Engineering Discovery Environment (ACM, New York, NY, USA)
- [24] Zirnstein, E. J., Heerikhuisen, J., Funsten, H. O., Livadiotis, G., McComas, D. J., Pogorelov, N. V. 2016, Astrophys. J. Lett., 818, L18

Table 1. Solar and interstellar plasma and magnetic field parameters used in multi-fluid MHD heliosphere simulation

Parameter	Value
Interstellar magnetic field strength B_{ism}	3 μG
Interstellar magnetic field direction	see Figure 1
Interstellar flow V_{ism}	26.4 km/s
Interstellar flow direction	see Figure 1
Interstellar ion density n_p	0.06 cm^{-3}
Interstellar neutral hydrogen density n_H	0.18 cm^{-3}
Fast solar wind speed V_f	762 km/s
Fast solar wind density at 1 AU n_f	2.4 cm^{-3}
Slow solar wind speed V_s	450 km/s
Slow solar wind density at 1 AU n_s	6.9 cm^{-3}
Heliospheric magnetic field at 1 AU $B_{1\text{AU}}$	47 μG

Table 2. Derived interstellar parameters for the distribution function of 5 TeV cosmic rays

Parameter	$A_{ 1}$	$A_{ 2}$	$ \nabla_{\perp} \ln f $	Direction of $\nabla_{\perp} \ln f$
Value	0.19%	0.037%	0.028%/R _g (370 AU)	see Figure 1

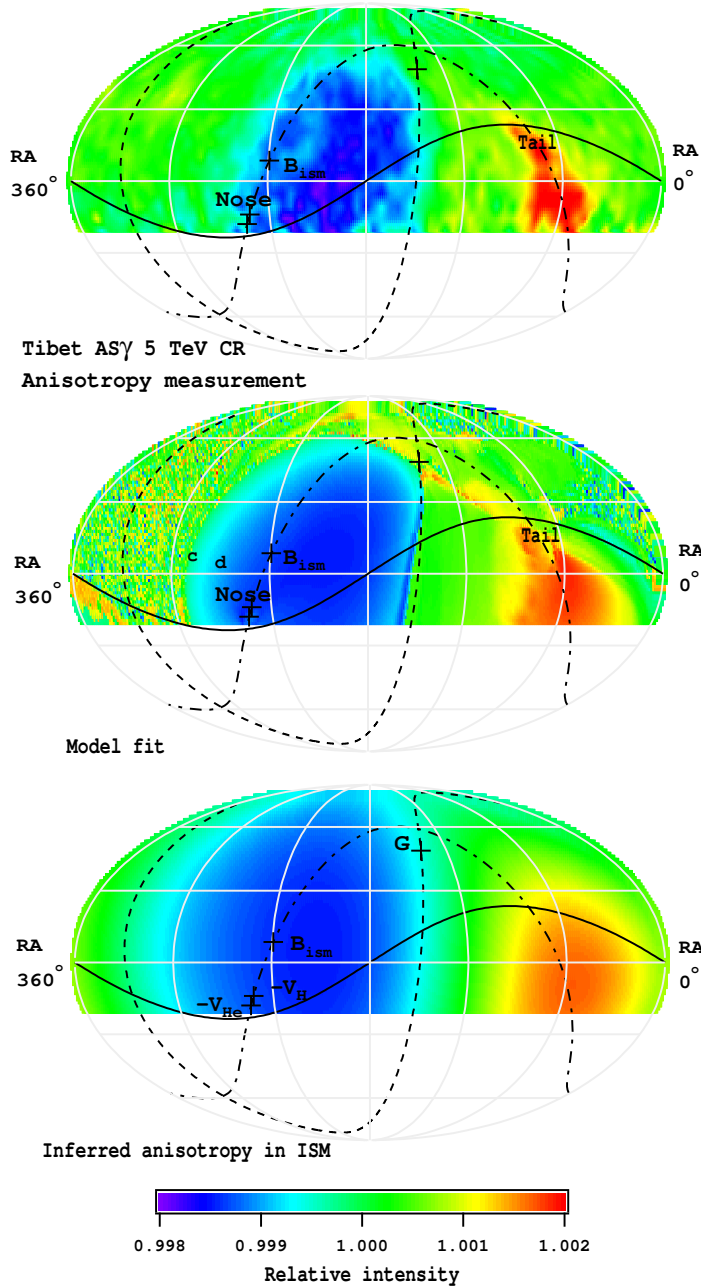


Figure 1. (Top) Tibet AS γ measurements of 5 TeV cosmic-ray relative flux as a function of declination and right ascension. (Middle) least χ^2 fit to Tibet measurements using Liouville mapping of anisotropy and the distribution function in Eq (2). (Bottom) inferred map of cosmic-ray anisotropy in the pristine interstellar anisotropy without the distortion by the heliosphere. The “+” signs indicate the direction of interstellar magnetic field \mathbf{B}_{ism} , the directions of interstellar neutral helium ($-\mathbf{V}_{He}$) and hydrogen ($-\mathbf{V}_H$) inflows, and the direction of perpendicular cosmic-ray density gradient G . The dot-dashed curve is the hydrogen deflection plane. The dashed curve is the plane perpendicular to the interstellar magnetic field \mathbf{B}_{ism} . The solid curve is the ecliptic. The sun is placed at the nose.

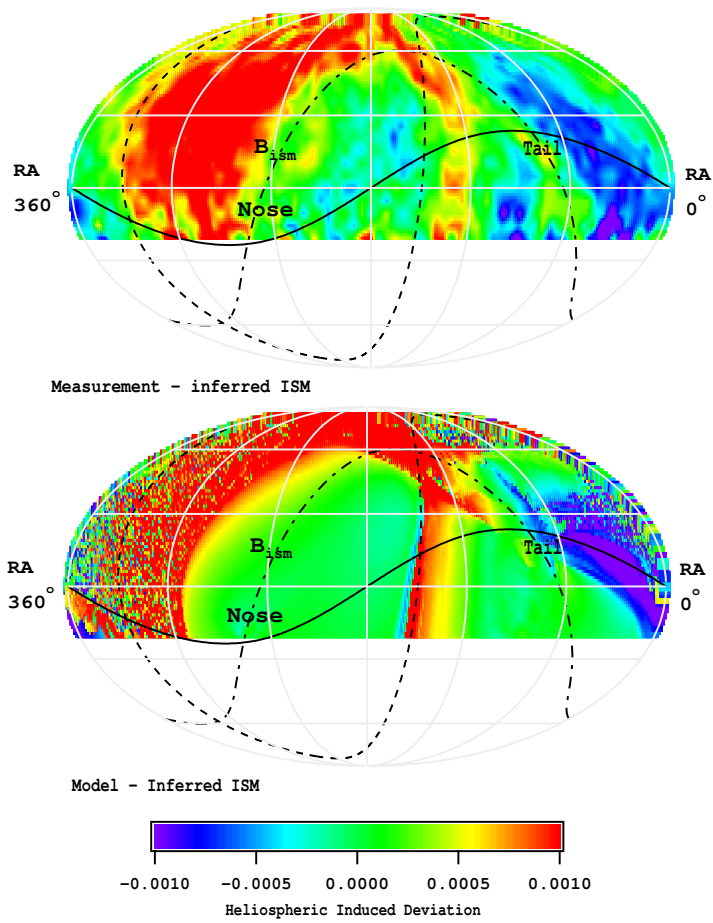


Figure 2. Distortion of cosmic-ray anisotropy caused by the heliosphere. The top is a map of Tibet AS γ measurements subtracted by the inferred interstellar anisotropy and the bottom is our model fit subtracted by the inferred interstellar anisotropy.

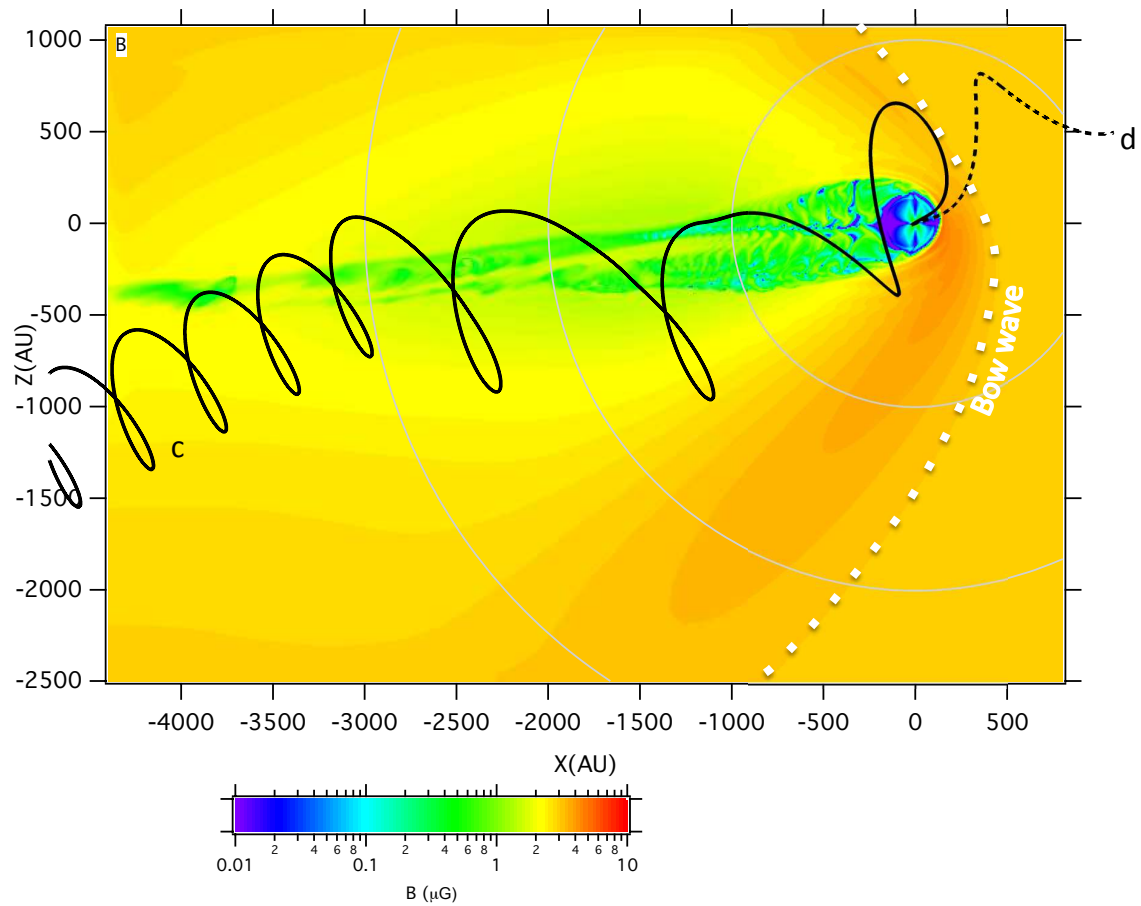


Figure 3. Magnetic field strength in the meridional plane. The two curves are the projections of sample cosmic-ray trajectories arriving in the directions “c” and “d” labelled in Figure 1 middle panel. The white dotted curve shows the location of heliosphere bow wave.

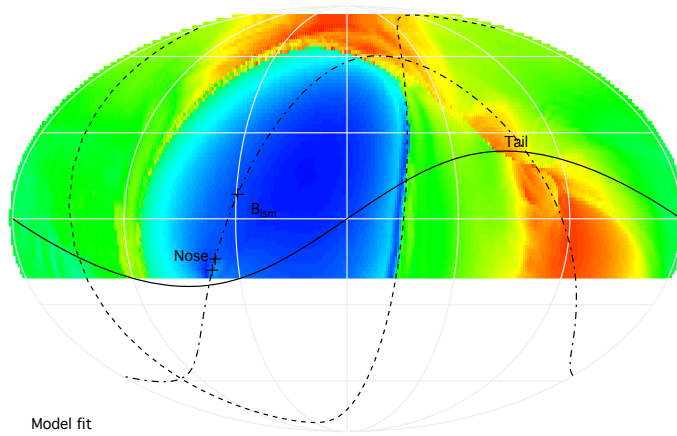


Figure 4. Model calculation of cosmic-ray anisotropy if the heliosphere is truncated and filled with the pristine interstellar magnetic field and flow beyond 2000 AU